Geometric Optimization of an Electrochemical Purification Cell to Prevent Corrosion in CSP Plants During Operation

Preprint

Kerry Rippy,[1,2] Liam Witteman,[3] Abigail Monasterial,[1] Patrick Taylor,[2] and Judith Vidal[1,2]

1 National Renewable Energy Laboratory
2 Colorado School of Mines
3 Mines/NREL Advanced Energy Systems Graduate Program

Presented at SolarPACES 2021
September 27-October 01, 2021

NREL is a national laboratory of the U.S. Department of Energy
Office of Energy Efficiency & Renewable Energy
Operated by the Alliance for Sustainable Energy, LLC

This report is available at no cost from the National Renewable Energy Laboratory (NREL) at www.nrel.gov/publications.

Contract No. DE-AC36-08GO28308

Conference Paper
NREL/CP-5500-80088
June 2022

Geometric Optimization of an Electrochemical Purification Cell to Prevent Corrosion in CSP Plants During Operation

Preprint

Kerry Rippy,[1,2] Liam Witteman,[3] Abigail Monasterial,[1] Patrick Taylor,[2] and Judith Vidal[1,2]

1 National Renewable Energy Laboratory
2 Colorado School of Mines
3 Mines/NREL Advanced Energy Systems Graduate Program

Suggested Citation
Rippy, Kerry, Liam Witteman, Abigail Monasterial, Patrick Taylor, and Judith Vidal. *Geometric Optimization of an Electrochemical Purification Cell to Prevent Corrosion in CSP Plants During Operation: Preprint*. Golden, CO: National Renewable Energy Laboratory. NREL/CP-5500-80088. https://www.nrel.gov/docs/fy22osti/80088.pdf.

NREL is a national laboratory of the U.S. Department of Energy
Office of Energy Efficiency & Renewable Energy
Operated by the Alliance for Sustainable Energy, LLC

This report is available at no cost from the National Renewable Energy Laboratory (NREL) at www.nrel.gov/publications.

Contract No. DE-AC36-08GO28308

Conference Paper
NREL/CP-5500-80088
June 2022

National Renewable Energy Laboratory
15013 Denver West Parkway
Golden, CO 80401
303-275-3000 • www.nrel.gov

NOTICE

This work was authored in part by the National Renewable Energy Laboratory, operated by Alliance for Sustainable Energy, LLC, for the U.S. Department of Energy (DOE) under Contract No. DE-AC36-08GO28308. Funding provided by the Mines/NREL Advanced Energy Systems Graduate Program. This work was also supported in part by the U.S. Department of Energy, Office of Science, Office of Workforce Development for Teachers and Scientists (WDTS) under the Science Undergraduate Laboratory Internships (SULI) program. The views expressed herein do not necessarily represent the views of the DOE or the U.S. Government. The U.S. Government retains and the publisher, by accepting the article for publication, acknowledges that the U.S. Government retains a nonexclusive, paid-up, irrevocable, worldwide license to publish or reproduce the published form of this work, or allow others to do so, for U.S. Government purposes.

Cover Photos by Dennis Schroeder: (clockwise, left to right) NREL 51934, NREL 45897, NREL 42160, NREL 45891, NREL 48097, NREL 46526.

Geometric Optimization of an Electrochemical Purification Cell to Prevent Corrosion in CSP Plants During Operation

Kerry Rippy[1,2, a)], Liam Witteman[3], Abigail Monasterial[1], Patrick Taylor[2], and Judith Vidal[1,2]

[1]*National Renewable Energy Laboratory, 15013 Denver West Parkway, Golden CO, 80401, USA*
[2]*Colorado School of Mines, 1500 Illinois St., Golden, CO, 80401, USA*
[3]*Mines/NREL Advanced Energy Systems Graduate Program, 1500 Illinois St., Golden, CO, 80301, USA*

[a)] Corresponding author: kerry.rippy@nrel.gov

Abstract. When exposed to moisture or oxygen, molten chloride salts produce corrosive impurities which degrade containment alloys.[1] This can significantly decrease the lifetime and increase costs of molten-salt-based systems.[2, 3] To overcome this barrier, we designed and modeled an electrochemical purification cell to remove the corrosive impurity $MgOH^+$. Various reactor architectures, including continuous stirred tank reactors (CSTRs) and plug flow reactors (PFRs) were investigated. Steady-state thermoelectric properties were evaluated using analytical methods, allowing assessment of the effects of structure and design parameters such as flow rate, cell length, and cross-sectional area of molten salt. The results suggest that our design could most effectively increase reliability and decrease costs of molten-chloride-salt-based systems by protecting them during continuous operation using an annular plug flow reactor.

INTRODUCTION

Concentrating Solar Power (CSP) stores thermal energy to generate renewable electricity on demand. The inclusion of storage is a major advantage, but CSP is still relatively expensive compared to other sources of electricity, such as photovoltaics. Therefore, the Department of Energy (DOE) has announced a target of 5¢/kWh for the levelized cost of energy (LCOE) of CSP systems.[4]

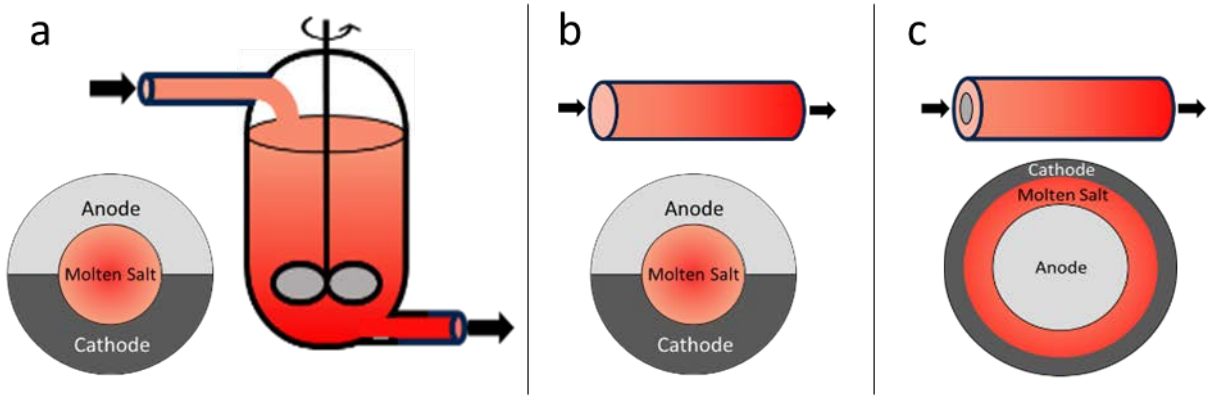

FIGURE 1. Schematic of the three reactor types evaluated by analytical modeling in this report. Cross sections of the reactors are included to show locations of anode, cathode, and molten salt. Drawings are not to scale. a) continuous stirred tank reactor (CSTR), b) plug flow reactor (PFR), and c) annular plug flow reactor (annular PFR). For the CSTR and PFR, the anode and cathode halves of the reactor would be separated with an insulating layer.

For CSP to meet the goals outlined by the DOE SunShot Initiative, the next generation of CSP plants (Gen3) will need to operate at a higher temperature than current heat transfer fluids are compatible with. For example, commonly used molten nitrate salts begin to decompose at 565°C. Molten chloride salts, in contrast, have much higher decomposition temperatures of up to 800°C. As a result, the DOE has supported efforts to develop and devise implementation plans for the ternary molten chloride salt NaCl-KCl-$MgCl_2$ as a possible heat transfer fluid in the Gen3 CSP plants. NaCl-KCl-$MgCl_2$ is stable above 800°C and relatively inexpensive,[2, 5] making it a promising candidate.

However, to keep containment cost low and component reliability high, corrosion problems associated with molten chloride salts must be addressed.[5] Corrosion in molten chloride salts is driven by hydroxide impurities.[6] Specifically, when exposed to air and moisture, MgCl reacts to form MgOHCl which ionizes to form corrosive $MgOH^+$. A procedure using melted metallic Mg can remove this corrosive species from the salt prior to use in the CSP plant. However, because the ternary chloride salt is strongly hygroscopic, corrosive impurity formation can occur during plant operation. [6] As reported in our previous work,[7] a potentially catastrophic amount of moisture ingress will occur during plant operation via the N_2 ullage gas, which has a nonzero water content. However, the Mg particle purification procedure cannot be used within the CSP plant, because it relies on temperatures above 650°C to melt the Mg, and the cold side of the next generation of CSP plant will be at 500°C. [4]

Therefore, we have devised a method for removal of $MgOH^+$ from CSP plants during operation. This method will consist of an electrochemical system with an Mg anode. An applied voltage in this cell will facilitate purification via electropositive Mg even at 500°C. This system will also employ a W cathode, which can stand up to the corrosive molten salt environment. This electrochemical system has been shown to control corrosion at the lab scale. The purification proceeds according to the following reactions:

$$2MgOHCl \rightarrow 2MgOH^+ + 2Cl^- \quad \textit{(occurs in molten salt)} \quad (1)$$

$$Mg(s) \rightarrow Mg^{2+} + 2e^- \quad \textit{(occurs at Mg anode)} \quad (2)$$

$$2MgOH^+ + 2e^- \rightarrow 2MgO + H_2(g) \quad \textit{(occurs at W cathode)} \quad (3)$$

$$Mg^{2+} + 2Cl^- \rightarrow MgCl_2 \quad \textit{(occurs in molten salt)} \quad (4)$$

This gives the net reaction:

$$2MgOHCl + Mg(s) \rightarrow MgCl_2 + 2MgO + H_2(g) \quad (5)$$

Note that the products of reaction (5) are not corrosive. MgO is a solid which can be filtered from the molten salt via in-line filtration, and H_2 will be swept out with the ullage gas, never building up to problematic levels.

To implement this electrochemical method in a CSP plant, it is neccessary to design a flow cell to purify salt. Specifically, we selected a reactor design based on parameters requried for a relatively small scale pilot plant, with a molten salt flow between 68-110 gal/min in 2" pipes, targeting an in-line reactor capable of purifying the entire throughput of salt in single pass in real time. The expected accumulation of impurity during plant operation, as well as the decision to utilize an in-line flow cell, have been discussed elsewhere.[7]

Several flow cell designs were considered as a part of this work. An initial downselection was made based on the feasibility of a given reactor type to be manufactured at necessary scales and its ability to withstand industrial conditions. Then, analytical models we used to predict the performance of each downselected reactor types. Specifically, we created analytical models for a continuous stirred tank reactor design (CSTR), a plug flow reactor design (PFR), and an annular plug flow design (annular PFR). A schematic of these reactor types is given in Fig. 1.

METHODS

Analytical Models for CSTR, PFR, and Annular PFR Reactors

It is possible to analytically solve the mass balance equations for CSTR and PFRs and extract valuable information on design parameters versus reactor performance. The analytical solutions for the CSTR, PFR, and annular PFR are summarized in Table 1.

In Table 1, $c_{MgOH^+,in}$ and $c_{MgOH^+,out}$ are the concentration of $MgOH^+$ going in and out of the reactor, respectively; D is the diameter of the molten-salt flow area, H is the height of the CSTR, L is the length of the PFRs, Q_{in} is the volumetric flow rate of the molten salt going into the reactor, k_m is the mass-transfer coefficient of $MgOH^+$ toward

TABLE 1. Concentration profiles derived from conservation of mass for various reactor types. Concentration profiles are evaluated in terms of the ratio of the concentration of the corrosive species, $MgOH^+$ exiting the purification cell to the concentration of $MgOH^+$ entering the cell. Lower values, indicating more removal of $MgOH^+$, are targeted.

	CSTR	PFR	Annular PFR
$\frac{c_{MgOH^+,out}}{c_{MgOH^+,in}} =$	$\frac{1}{1+\frac{\pi DHk_m}{2Q_{in}}}$	$exp\left(\frac{-2Lk_m}{Dv}\right)$	$exp\left(\frac{-4D_{outer}Lk_m}{(D_{outer}^2-D_{inner}^2)v}\right)$

the cathode surface, v is the velocity of the molten salt going into the reactor, and D_{outer} and D_{inner} are the outer and inner diameter of the annular PFR, respectively.

The one intrinsic system parameter, the mass-transfer coefficient, is a parameter that can be readily calculated from well-established correlations in the literature.[8-11] The molten-salt properties and diffusion data for the calculations was taken from previous reports.[12, 13] From Table 1, it is possible to predict the outlet concentration of $MgOH^+$ based on the inlet concentration, reactor dimensions, and flow rate. The main assumptions are that reaction of $MgOH^+$ to form MgO at the cathode does not alter the molten-salt flow rate and that the reactor is at steady state. The reactor performance is assessed on its effectiveness of $MgOH^+$ removal, i.e., the ratio of $c_{MgOH^+,out}$ to $c_{MgOH^+,in}$ should be minimized. For calculations utilizing these equations, we generally assume the starting concentration of $MgOH^+$ to be 1 mol % and the reactor to be isothermal at 500 °C.

To illustrate our methods, we will give a more detailed discussion of the reactor modeling theory for one of the three reactor types, the annular PFR reactor.

If we assume $c_{MgOH^+}$to vary only in the direction of the flow (plug flow) then the concentration profile can be derived from the conservation of mass equation. The resulting concentration profile for flow in an annulus is:

$$\frac{c_{MgOH^+,out}}{c_{MgOH^+,in}} = \exp\left(-\frac{-2Lr_{cat}k_m}{v(r_{cat}^2-r_{an}^2)}\right) \quad (6)$$

Where L is the length of the reactor, D_{cat} is the diameter of the cathode (outer diameter), D_{an} is the diameter of the anode (outer diameter), k_m is the mass transfer coefficient towards the cathode, and v is the velocity of the molten chloride salt.

The relation between D_{cat} and D_{an} can be written as:

$$r_{an} = \kappa r_{cat} \quad (7)$$

Where κ is the ratio of inner to outer diameter.

The mass transfer coefficient, k_m, can be calculated using the Chilton-Colburn j-factor analogy for mass transfer, which has been shown to fit data well for diffusion limited process in annular flow between 2 concentric electrodes.[11]

$$j_M = \frac{k_m}{v}Sc^{2/3} = \frac{f}{2} \quad (8)$$

Where j_M is the Chilton-Colburn j-factor analogy for mass transfer, Sc is the Schmidt number, and f is the friction factor.

The friction factor for an annulus at various κ has been established for laminar and turbulent flow:[9, 14]

$$f_{laminar} = \frac{16}{Re_\kappa} \quad (9)$$

$$\sqrt{\frac{1}{f_{turbulent}}} = G \cdot \log_{10}\left(Re_\kappa\sqrt{f}\right) - H \quad (10)$$

$$Re_\kappa = K \cdot \frac{2r_{cat}(1-\kappa)v\rho}{\mu} \quad (11)$$

Where Re_κ is the Reynolds number, ρ is the molten salt density, μ is the molten salt viscosity, and G, H, and K are constants as a given of κ. Literature values for thermophysical properties of the ternary chloride salt from Wang et al[12] have been used.

$$\mu = 0.70645 \cdot \exp\left(\frac{1204.11348}{T+273.15}\right) \quad (12)$$

Where μ is in units of cP, and T in °C.

$$\rho = 1958.8438 - 0.56355 \cdot T \tag{13}$$

Where ρ is in units of kg/m^3, and T in °C.

The Schmidt number is a dimensionless number defined as,

$$Sc = \frac{\mu}{\rho \mathcal{D}_{MgOH^+}} \tag{14}$$

Where $\mathcal{D}_{MgOH^+}$ is the diffusion coefficient of $MgOH^+$.

The diffusion coefficient can be estimated from the Stoke-Einstein equation.[9]

$$\mathcal{D}_{MgOH^+} = \frac{kT}{6\pi\mu R_{MgOH^+}} \tag{15}$$

Where k is the Boltzmann constant 1.380x10^{-23} J/K, and $R_{MgOH^+}$is the ionic radius of the molecule $MgOH^+$. No data could be found for the ionic radius, so it was grossly estimated by adding the ionic radius of Mg^{2+} (0.65 Å) and OH^- (1.33 Å).

Finally, the discussion so far assumed the effective mass transfer area to be the entire wetted perimeter. In our system, only the cathode mass transfer area participates in the purification reaction, so an area correction factor is applied.

$$k'_m = k_m \cdot \frac{A_{cat}}{A_{cat} + A_{an}} \tag{16}$$

Using the above, we were able to find an analytical solution for the purification of the molten chloride salts utilizing the annular PFR reactor.

Electrode Spacing Calculation for Annular PFR Approaching Slit Flow

The main concern of the lower limit of electrode spacing is that wall forces start to dominate over the fluid's inertia, i.e. capillary flow. The dimensionless number that characterizes the ratio of viscous forces over surface tension is the capillary number.

$$Ca = \frac{\mu v}{\sigma} \tag{17}$$

Where μ is viscosity, v is velocity, and σ is surface tension.

Furthermore, the Reynolds number characterizes the ratio of inertia over viscous forces. Multiplying Ca by Re results in the Weber number, which characterizes the ratio of inertia over surface tension.

$$We = ReCa = \frac{\mu v}{\sigma} \cdot \frac{\rho v D_e}{\mu} = \frac{\rho v^2 D_e}{\sigma} \tag{18}$$

Where ρ is density, and D_e is the equivalent diameter.

The equivalent diameter is four times the hydraulic radius, which is calculated as:

$$D_e = 4r_h = 4\frac{S}{L_p} = 4\frac{\delta H}{2(\delta + H)} = 2\frac{\delta H}{(\delta + H)} \tag{19}$$

Where S is the cross-sectional area of the channel, and L_p is the length of the wetted perimeter.

It is apparent from (2) that as electrode spacing decreases, D_e decreases and therefore We decreases.

Another limitation is that as electrode spacing decreases, friction/pressure drop increases and therefore pumping cost goes up.

The pressure drop due to skin friction between the fluid and the wall is expressed as:

$$\frac{\Delta p_s}{L} = \frac{2f\rho\bar{V}^2}{D_e} \tag{20}$$

Where Δp_s is the pressure drop due to skin friction, L is the length of the channel, f is the fanning friction factor, and $\bar{V}^2$ is the average fluid velocity in the channel.

From the Hagen-Poiseuille equation the friction factor for laminar flow is

$$f = \frac{16}{Re} \tag{21}$$

For flow between parallel plates the critical Reynolds number signifying laminar-turbulent transition is 2285.

The friction factor for turbulent flow is

$$f = 0.0014 + \frac{0.125}{Re^{0.32}} \tag{22}$$

The amount of work required for a pump can be calculated through the Bernoulli equation.

$$\frac{p_a}{\rho} + gZ_a + \frac{\alpha_a \bar{V}_a^2}{2} + \eta W_p = \frac{p_b}{\rho} + gZ_b + \frac{\alpha_b \bar{V}_b^2}{2} + h_f \quad (23)$$

Where p is pressure, g is the gravitational acceleration, Z is height, α is the kinetic correction factor, η is the efficiency of the pump, W_p is the work done by the pump, and h_f is the loss due to fluid friction.

The fluid friction energy loss can be related to the friction factor according to:

$$h_f = \frac{2fL\bar{V}^2}{D} \quad (24)$$

Furthermore, there will be friction loss from sudden expansion and contraction of the channel. These two losses are expected since the pipe going into and out of the reactor will be 2" as seen in Figure 2.

The friction loss from sudden expansion is expressed as:

$$h_{fe} = K_e \frac{\bar{V}_a^2}{2} \quad (25)$$

Where K_e is the expansion loss coefficient, and $\bar{V}_a$ is the average velocity in the smaller upstream channel.

The expansion loss coefficient can be calculated as:

$$K_e = \left(1 - \frac{S_a}{S_b}\right)^2 \quad (26)$$

Similarly, the friction loss from sudden contraction is expressed as:

$$h_{fc} = K_c \frac{\bar{V}_b^2}{2} \quad (27)$$

Where K_c is the contraction loss coefficient, and $\overline{V_b}$ is the average velocity in the smaller downstream channel.

The contraction loss coefficient is given by the empirical expression:

$$K_c = 0.4(1 - \frac{S_b}{S_a}) \quad (28)$$

The kinetic correction factor is 2.0 for laminar flow and for turbulent flow can be calculated using the friction factor.

$$\alpha = 1 + 0.78f(15 - 15.9\sqrt{f}) \quad (29)$$

The pump power to overcome the skin friction loss can be calculated as:

$$P = \frac{\dot{m}h_f}{\eta} \quad (30)$$

Where $\dot{m}$ is the mass flow rate, and η is the pump efficiency. Thus, it is possible to calculate the pump efficiency and correlate it to electrode spacing.

RESULTS AND DISCUSSION

Many reactor designs were considered for the electrochemical purification cell. Complex design features in some cases offered performance advantages, the priority placed on cost eliminated them. For example, the electrochemical removal of the corrosive impurity $MgOH^+$ occurs at the cathode surface. Thus, a high surface area is desirable. To increase surface area, mesh electrodes were considered. However, for this system cathode is made of W which is difficult to machine, and the use of W mesh would have resulted in prohibitively high cost. Similarly, complex shapes for the Mg anode were considered, to encourage dissolution of more Mg^{2+} into solution according to reaction (2). However, complex shapes would be more likely to fail and break apart as Mg dissolved. Furthermore, specialized complex shapes would be more expensive to replace regularly. Thus, a priority was placed on reactor designs that utilize commercially available pipes and rods.

Preliminary downselection to three different flow reactor types was thus achieved. These three types, illustrated in Fig. 1, were the CSTR, PFR, and annular PFR. To evaluate and compare reactor types, the performance of the CSTR and PFR was assessed as a function of flow rate and pipe diameter assuming a fixed reactor length of 10 m and a fixed initial impurity concentration of 1 mol %, which we considered the upper level of acceptable $MgOH^+$

concentration that should be allowed to form before being reduced by the purification cell. The results are shown in Fig. 2. Analytical models, discussed in the methods section above, were utilized.

From Fig. 2, higher flow rates resulted in reduced reactor performance, which is attributed to lower residence time in the reactor. Also, smaller pipe diameters resulted in better reactor performance, largely because of the greater electrode area to reactor volume ratio. However, at these conditions both the the CSTR and PFR perform poorly. At a flow rate of just 1 gal/min and a pipe diameter of 10 cm, the $MgOH^+$ concentration was only reduced from 1 mol% to 0.975 mol%.

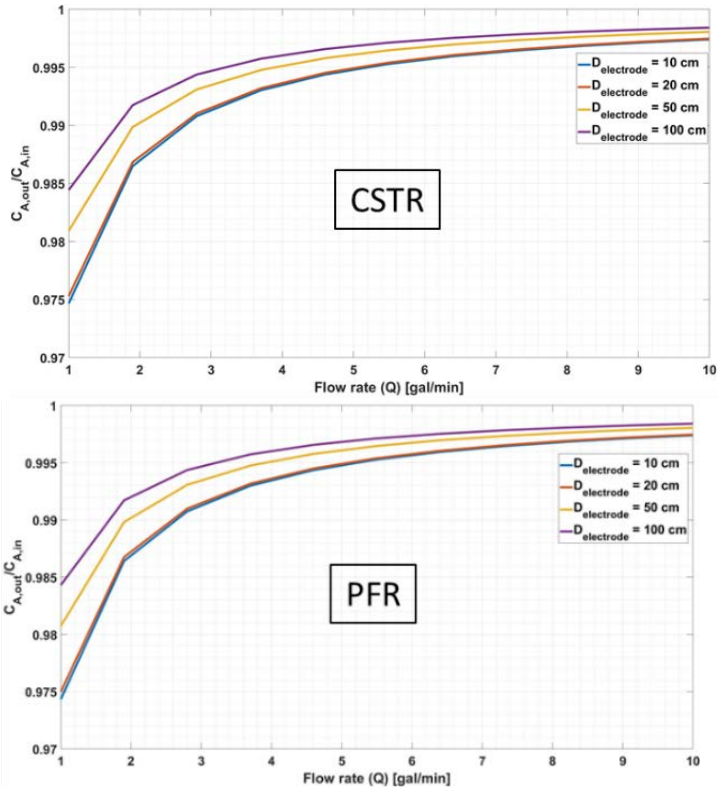

FIGURE 2. Reactor performance versus pipe diameter and flow rate.

Based on the results from Fig. 2, both the CSTR and PFR would require either impractically large size or prohibitively slow flow rates to be effective. For example, to achieve a 90% reduction in $MgOH^+$, ensuring $MgOH^+$ concentration does not continually build up over time,[7] a length of 3.462 km would be required for the CSTR, and 0.886 km for the PFR, even at the untenably slow flow rate of 1 gal/min and a pipe diameter of 10 cm. Reactors on the km length scale are clearly not feasible from a cost perspective.

Thus, the annular PFR design was prioritized. Its performance was assessed similarly to the above analysis for the CSTR and PFR, except with the anode diameter fixed at 10 cm and the cathode diameter varied, giving a variable distance between the anode and cathode. The results are shown in Fig. 3.

From Fig. 3, the reactor performance significantly improves when an annular PFR is considered, especially as the outer diameter approaches the inner diameter, i.e. better performance as the two electrode surfaces approach each other. This is not surprising, as this condition maximizes the ratio of electrode surface area to reactor volume, and purification occurs at the electrode surface.

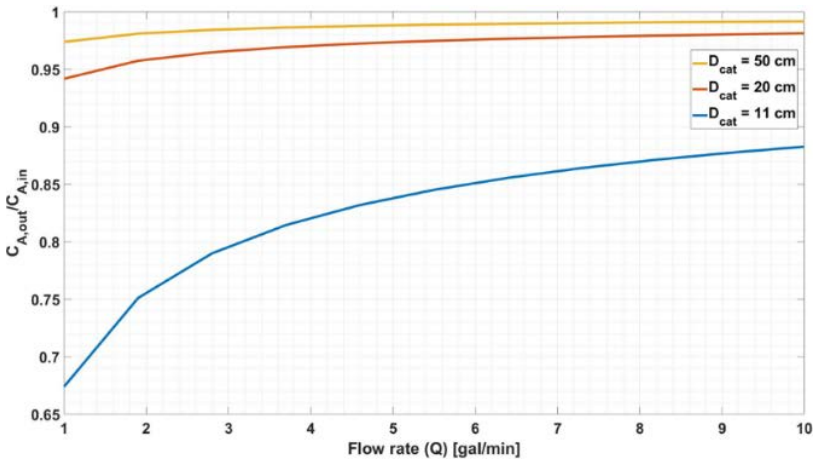

FIGURE 3. Annular PFR reactor performance versus outer pipe diameter.

Applying the same calculation to the annular PFR that was used for the CSTR and PFR, we found that a length of 0.058 m would be required for 90% reduction of $MgOH^+$ under the specified conditions. Thus, we concluded that, utilizing the metric of length required to purify salt, an annular PFR is approximately one order of magnitude more effective than a PFR and two orders of magnitude more effective than a CSTR.

We therefore further optimized the annular PFR system, by continuously decreasing the diameter of the outer electrode. Ultimately, we found that the best purification was achieved when slit flow was approached, i.e. when the distance between anode and cathode became so small that the salt flow could be modeled as slit flow between two parallel plates. In fact, we calculated that for an electrode spacing of 1 cm, a reactor length of only 9 m was required.

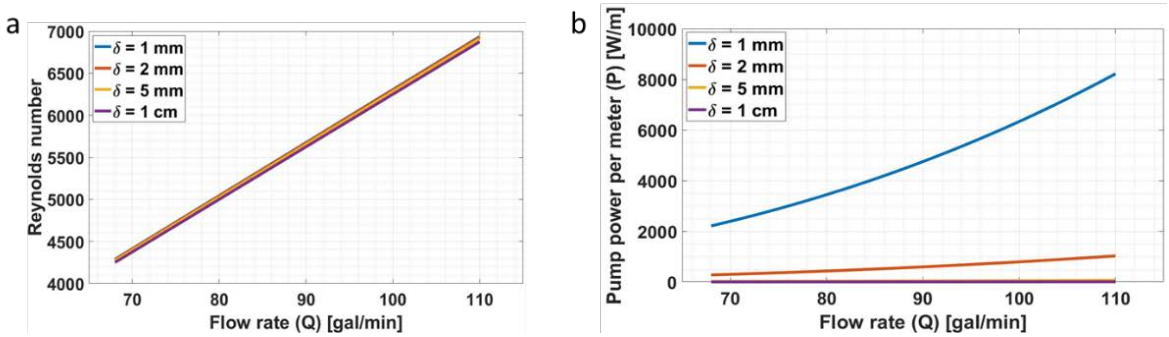

FIGURE 4. a) Reynolds number as a function of flow rate and electrode spacing and b) The increased pump power to overcome friction loss at various electrode spacings.

To ensure feasibility of the annular reactor with slit flow, the friction factor for flow between the electrodes was calculated across the relevant Reynolds number range associated with the flow rate. Calculations were performed according to the equations discussed in the methods section above. The resulting Reynolds number is given as a function of spacing between electrodes in Fig. 4(a). We found that friction losses would not become significant until a spacing of around 2 mm or less was reached. Note that in Fig. 4(b), at a spacing of 2 mm only a small increase in required pump power is observed, whereas at 1 mm, significantly increased power is required. Thus, we determined that an annular PFR is both a preferred and feasible reactor design.

CONCLUSIONS

Idealized chemical reactor designs were utilized to derive analytical expressions for the concentration of corrosive $MgOH^+$ entering and exiting CSTR, PFR, and annular PFR purification reactors. We found that each successive design (CSTR → PFR → annular PFR) showed order of magnitude improvement, moving from a reactor length over 1 km long to meters long. Thus, the annular PFR design is preferred. We also note the advantage of the annular PFR from a cost and manufacturing standpoint. The PFR is composed of a W pipe and a Mg rod, which are both readily

available. In contrast, the CSTR and PFR would require an airtight, insulating seal between the anode and cathode portions of the pipe, which would be difficult and expensive to achieve.

ACKNOWLEDGMENTS

This work was supported by DOE SETO grant CPS #35931 and the Mines/NREL Advanced Energy Systems Graduate Program. We also thank Sridhar Seetharaman, Matthew Earlam, and Stephen James.

REFERENCES

1. J. C. Gomez-Vidal and R. Tirawat, Solar Energy Materials and Solar Cells **157**, 234-244 (2016).
2. W. Ding, H. Shi, A. Jianu, Y. Xiu, A. Bonk, A. Weisenburger and T. Bauer, *Solar Energy Materials and Solar Cells* **193**, 298-313 (2019).
3. W. Ding, A. Bonk, J. Gussone and T. Bauer, Energy Procedia **135**, pp. 82-91 (2017).
4. M. Mehos, C. Turchi, J. Vidal, M. Wagner, Z. Ma, C. Ho, W. Kolb, C. Andraka and A. Kruizenga, *Concentrating Solar Power Gen3 Demonstration Roadmap*. (2017).
5. W. Ding, J. Gomez-Vidal, A. Bonk and T. Bauer, Solar Energy Materials and Solar Cells **199**, 8-15 (2019).
6. J. C. Gomez-Vidal and R. Tirawat, Medium: ED; Size: pp. 234-244 (2016).
7. K. Rippy, E. Howard, L. Witteman and J. Vidal, Solar 2021 Proceedings (2021).
8. J. B. Rawlings and J. G. Ekerdt, *Chemical Reactor Analysis and Design Fundamentals*. (2013).
9. R. B. Bird, W. E. Stewart and E. N. Lightfoot, *Transport Phenomena*. (Wiley, 2006).
10. D. A. Shaw and T. J. Hanratty, **23** (1), 28-37 (1977).
11. C. S. Lin, E. B. Denton, H. S. Gaskill and G. L. Putnam, Industrial & Engineering Chemistry **43** (9), 2136-2143 (1951).
12. X. Wang, J. D. Rincon, P. Li, Y. Zhao and J. Vidal, J. Sol. Energy Eng. (2019).
13. J. Guo, N. Hoyt and M. Williamson, Medium: X; Size: Article No. 115064 (2021).
14. M. Jack, T. W. Jackson, K. R. Purdy, C. C. Oliver, H. L. Johnson, W. Technical, D. M. Meter and R. B. Bird, *Flow in Annuli*. (1954).